Journal of Catalysis 260 (2008) 17–29

Contents lists available at ScienceDirect

Journal of Catalysis

www.elsevier.com/locate/jcat

Highly active and selective Nb modified MCM-41 catalysts for Beckmann rearrangement of cyclohexanone oxime to ε-caprolactam

M. Anilkumar, W.F. Hölderich *

Department of Chemical Technology and Heterogeneous Catalysis, RWTH Aachen University, Worringerweg 1, 52074 Aachen, Germany

ARTICLE INFO

Article history:
Received 1 July 2008
Revised 25 August 2008
Accepted 27 August 2008
Available online 16 October 2008

Keywords:
Beckmann rearrangement reaction
Gas phase reaction
Nb-MCM-41
Cyclohexanone oxime
ε-Caprolactam

ABSTRACT

The niobium incorporated MCM-41 molecular sieves (Si/Nb-16, 32, 64 and 128) have been synthesized by hydrothermal method using tetradecyltrimethyl ammonium bromide as templates in the absence of auxiliary organics. A combination of various physical techniques was used for characterizing the catalysts, such as X-ray diffraction, N_2 physisorption, diffuse reflectance UV–Vis (DR–UV–Vis), Fourier transmission infra red (FT-IR), atomic emission spectroscopy (ICP-AES), and ^{29}Si MAS NMR (magic-angle spinning nuclear magnetic resonance) spectroscopy. Catalyst acidity was measured by (ammonia temperature programmed desorption) NH_3-TPD and pyridine FT-IR techniques. The characterization results of DR–UV–Vis, FT-IR, and Si MAS NMR techniques confirm that Nb atoms are isolated and tetrahedrally coordinated in the framework of MCM-41. All the materials exhibit hexagonal arrangement of uniform mesopores. Structural characterization results revealed that two types of Nb oxide species are present, one is framework, and second one is surface type Nb species in all Nb-MCM-41 catalysts. Catalyst samples with higher loading of Nb have shown very good activity. The optimum temperature for this Beckmann rearrangement is 300 °C. The cyclohexanone oxime conversion was about 100% and a caprolactam selectivity of about 95% and more could be achieved. The effect of Si/Nb ratio, temperature, space velocity, etc., on catalyst activity, product selectivity and catalyst stability were discussed. The cyclohexanone oxime conversion was dependent on the temperature and space velocity. The activity at 300 °C for the various catalysts followed the order Nb-MCM-41(Si/Nb-16) > Nb-MCM-41(Si/Nb-32) > Nb-MCM-41(Si/Nb-64) > Nb-MCM-41(Si/Nb-128).

1. Introduction

The Beckmann rearrangement of cyclic ketooximes to lactams is an important process step for production of polyamides. For example, Beckmann rearrangement of cyclohexanone oxime (CHO) produces ε-caprolactam (CL), which is an important monomer for synthesis of Nylon-6 polyamide. On an industrial scale, CL is produced in liquid phase reaction conditions by using stoichiometric amounts of concentrated sulfuric acid and oleum as catalyst. This method has several disadvantages such as the corrosion of the reactors and the formation of ammonium sulfate as a by-product resulting from the neutralization of sulfuric acid with ammonia [1–3]. Consequently, to overcome these problems, more economic and environmentally friendly process technology has been developed in the gas phase Beckmann rearrangement reaction using solid acid catalysts [4,5]. Previous studies showed that solid acids such as tungsten oxide [6], silica-tantalum oxide [7], titanium oxide [8], and boron-silica [9] are active catalysts. However, the application of all these catalysts resulted in low selectivity for CL and exhibited fast deactivation for the reaction. Recently, zeolites as solid acid catalysts for Beckmann rearrangement reaction have been used [2,3,10–13]. Several potential materials along with all these materials such as TS-1 [14], SAPO 11 [15], Beta, Y [10,16,17], ZSM-5 [10,11,17–19], and monolithic zeolite [20] catalysts were applied for this reaction under gas phase as well as in liquid phase conditions. In addition, mesoporous Si-MCM-41 and Al-MCM-41 molecular sieves also lead to promising results [21]. Particularly, our group observed specially modified high silica B-MFI zeolite is a very active and selective catalyst for gas phase Beckmann rearrangement reaction in a fluidized bed reactor [2,3,22,23]. Sumitomo Chemicals Co. Ltd has carried out a lot of gas phase investigations in the presence of silicalite zeolites [11–13,24–26]. Currently, they have commercialized such a process and are producing 60,000 t of CL per year by this method [13]. A review article by Hölderich et al. gives an extensive outline of the Beckmann rearrangement technologies [3].

Nb incorporated MCM-41 catalysts were first reported by Ziolek and Nowak [27]. These catalysts are very active for oxidation of organic compounds under mild conditions [28], epoxidation of organic compounds [29], hydrodesulfurization and hydrogenation [30] reactions. Also, other materials containing Nb have shown high activity in esterification, oxidative dehydrogenation, and alky-

* Corresponding author. Fax: +49 2418022291.
E-mail address: hoelderich@rwth-aachen.de (W.F. Hölderich).

0021-9517/$ – see front matter © 2008 Published by Elsevier Inc.
doi:10.1016/j.jcat.2008.08.019

lation of aromatic compounds [31]. From the above examples, it is very clear that niobium has significant effect in heterogeneous catalysis research for synthesis of chemicals.

Recently, Jung et al. observed that silica supported mesoporous Nb and Ta catalysts are active for cyclohexanone oxime conversion and caprolactam selectivity in gas phase Beckmann rearrangement reaction [32]. Present work deals with highly ordered, niobium incorporated MCM-41 samples with different pore diameters and different niobium concentrations and their evaluation for Beckmann rearrangement of cyclohexanone oxime under gas phase conditions. Various characterization techniques such as nitrogen physisorption, XRD, FT-IR, UV-DIR, NH_3 TPD, pyridine FT-IR and ^{29}Si NMR were used to characterize the physicochemical properties of Nb-MCM-41 catalysts. The physical properties of Nb-MCM-41 catalysts during the Beckmann rearrangement reaction were investigated as well. When transition metal atoms were incorporated into MCM-41 materials, some active defects were generated. The role of defects formed after the incorporation of transition metal atoms into MCM-41 on the catalytic performance was investigated. The relation of catalyst acidity with activity was also examined. Nb-MCM-41 applied for rearrangement of CHO reaction was reported in a previous communication [32]. However, the effect of different reaction parameters such as temperature, WHSV, Si/Nb ratios and catalyst lifetime were not examined in this work. Also, catalyst characterization results were insufficient to determine whether Nb has incorporated into the mesoporous silica framework or not. In addition the selectivity and conversion need still to be improved in the paper of Jung et al. [32]. Hence, in this study we report detailed characterization and catalytic activity evaluation of Nb-MCM-41.

2. Experimental

2.1. Synthesis of Nb-MCM-41

Nb incorporated MCM-41 (Si/Nb-16-128) molecular sieves were synthesized based on the synthesis procedure of Vetrivel and Pandurangan [33]. Sodium meta silicate (ROTH, Germany) and niobium pentachloride (Fluka) were used as sources for silica and niobium, respectively. Tetradecyltrimethyl ammonium bromide was used as the structure-directing agent (Fluka). The molar compositions of the synthesis gel were as follows: SiO_2:$x$$NbCl_5$:0.2TDTAB:0.89$H_2SO_4$:120H_2O (x varies with Si/Nb ratio). Four samples with different Si/Nb ratios of 16, 32, 64, and 128 were synthesized. All the samples were dried at 110 °C for 12 h and calcined at 550 °C for 6 h.

2.2. Characterization

Powder X-ray diffraction (XRD) data were recorded on a Siemens diffractometer (D 5000) operated at 45 kV and 40 mA, using Nickel filtrated Cu$K\alpha$ radiation with 1.5406 Å between 1.5° and 40° (2 theta), with a scanning speed of 0.02°/min. Nitrogen adsorption isotherms were obtained at 77 K on a Micromeritics ASAP 2010 Gas Sorption and Porosimetry System. Samples were activated at 300 °C for 3 h under vacuum, and then the adsorption–desorption was conducted by passing nitrogen into the sample, which was kept under liquid nitrogen. Brunauer–Emmett–Teller surface areas were determined over a relative pressure range from 0.05 to 0.20.

Pore size distributions were calculated from the adsorption branch of the isotherms using the Barrett–Joyner–Halenda method. Bulk elemental analyses were measured with inductive couple plasma atomic emission spectroscopy (ICP-AES) on a spectroflame D (Spectro Analytic Instrument). Diffuse-reflectance UV–Vis spectra of solid samples were recorded with a Perkin Elmer Lambda 950 equipped with diffuse-reflectance attachment, with $BaSO_4$ as the reference. FT-IR spectra of samples were taken in the range of 4000–400 cm^{-1} on a Nicolet Protégé 460. The solid-state ^{29}Si MAS NMR spectra were recorded on a Bruker DSX 500 NMR spectrometer equipped with a 4-mm MAS probe head. The samples were spinning (MAS) at a rate of approximately 10 kHz. The spectra were recorded with a 45° pulse, a contact time of 10 s and a recycle delay of 5000 μs, without cross polarization. Sample spectra were deconvulated by dmfit 2008 software.

TGA–DTA measurements of spent catalyst were carried out on a Netzsch 209/2/E equipped with a STA-409 controller with an alumina plate under an air atmosphere (air flow) from ambient temperature to 1000 °C at a heating rate of 10 °C/min. XPS analysis of spent catalyst was measured in an Ultra Axis spectrometer. The samples were irradiated with monoenergetic Al$K\alpha_{1,2}$ radiation (1486.6 eV) and the spectra were taken at a power of 144 W (12 kV × 12 mA).

2.3. Surface acidity measurements

Acidity of the samples was measured with pyridine adsorbed FT-IR spectroscopy (Nicolet Protégé 460) equipped with an evacuable furnace cell with KBr windows, containing a sample wafer. Initially, catalyst powder was pressed into a 5 mm wafer, which was loaded into the IR chamber and heated up 400 °C over night under reduced pressure of 10^{-3} mbar. After the cell was cooled down to 50 °C the background spectra were recorded. Spectra were always collected as an average of 200 runs with 0.5 cm^{-1} definition. The pyridine adsorption was carried out slowly where the catalyst was equilibrated with pyridine vapors at 50 °C. After 60 min evacuation, a spectrum was recorded and heated stepwise scanning with IR spectroscopy.

NH_3-TPD of samples was measured on a TPDRO 1100 apparatus from CE instrument, with thermal conductive detector (TCD). Initially, samples were heated at 500 °C under inert gas for removal of physisorbed water from the catalysts. Afterwards, NH_3 was physisorbed from room temperature to 600 °C. The amount of desorbed ammonia was recorded by a thermal conductive detector (TCD) during various temperature scans.

2.4. Beckmann rearrangement reaction

The catalytic reaction was carried out in a fixed-bed reactor (316 stainless, 6 mm outer diameter). A mixture of pelletized Nb-MCM-41 (ca. 1.6–1.0 mm mesh) and quartz sand (also 1.6–1.0 mm mesh) was packed into the reactor, and then heated in flowing air at 500 °C for 4 h. Subsequently, the reactor was cooled to the desired reaction temperature. Before starting the reaction nitrogen gas was passed through catalyst bed for 15 min. CHO was dissolved in ethanol. The feed was injected into the reactor by a piston pump (Telab, Heidelberg) along with N_2 as carrier gas. The reactor outlet was connected to a cooling trap, which was immersed into an isopropanol and dry ice mixture. The reactor effluent taken at specified intervals was analyzed using a Siemens Chromatograph 5890, equipped with a flame ionization detector and a capillary column (FS-OV 1701, 50 m) with methyl undecanoate as the internal standard. Regeneration of the catalyst was done by calcination at 500 °C for 4 h under airflow. Reactions were performed with Design Expert-5 (Start-Ease) [34] and afterwards we followed the thereby optimized conditions.

3. Results and discussion

3.1. Characterization of the catalysts

3.1.1. Chemical analysis

Table 1 exhibits the material composition based on ICP analysis after calcinations at 500 °C. The data clearly show that the amount

Table 1
Physical properties of Nb-MCM-41 molecular sieves.

Catalyst	Si/Nb gel ratio	ICP	d_{100} (Å)	a_0 (Å)	BET surface area (m^2/g)	Pore volume (cm^3/g)	Pore diameter (Å)	Wall thickness (Å)
A	16	15.54	33.98	39.24	417	0.28	24.64	14.6
B	32	28.31	49.08	56.67	612	0.26	30.48	26.18
C	64	54.72	41.67	48.12	632	0.36	23.68	24.44
D	128	121.66	38.08	43.97	929	0.94	29.27	14.25

of metal after calcination is close to the expected values. It has been indicated in previous work that the amount of metal incorporated into the framework is mostly dependent on the type of silica source used in the synthesis procedure. When sodium silicate was used as the siliceous source, a higher amount of niobium was incorporated in the framework [35].

3.1.2. X-ray diffraction and low temperature nitrogen adsorption

The XRD patterns of Nb-MCM-41 sample after calcination show the hexagonal MCM-41 phase in the sample (Fig. 1). A typical low angle X-ray diffraction of MCM-41 shows 4 peaks, the first intensive peak appears approximately at $2\theta = 2°$ (miller indices 100) and other three peaks appear at $2\theta = 3–8°$ (miller indices 110, 200 and 210) [36]. In case of Nb incorporated MCM-41 molecular sieves, the XRD peaks of the calcined samples exhibit an intense signal at about 1.9–3° and an additional peak at 3.5–5° (miller indices 100, 110) with low intensity, while other peaks did not appear. The disappearance of miller indices 200 and 210 in the calcined samples may be due to the reduction of structure organization during the calcinations [37].

After calcination the peak positions shifted to higher 2θ values due to pore size contraction. Furthermore, the absence of diffractions at higher 2θ range corresponding to metal oxides indicated that metal ions were either well dispersed in the framework of MCM-41 or attained an amorphous form outside of the framework. The characterization techniques XRD and BET show that all the materials had the well-ordered hexagonal mesoporous structure of MCM-41 type with one system of pores (around 4 nm pore diameter) and very high surface area (1000 m^2/g). Table 1 summarizes the d_{100} spacing and lattice parameter (a_0) calculated as per literature from XRD and low-temperature nitrogen adsorption isotherms experiments. It can be seen that, upon introducing the Nb metal into the mesoporous MCM-41, the unit cell parameter calculated by $a_0 = 2d_{100}/\sqrt{3}$ and $d_{(100)}$ increased. It could be due to the larger ionic radius of Nb^{+5} (0.64 Å) and longer Nb–O bond length (1.69 Å). However, a decrease of the unit cell parameter and $d_{(100)}$ spacing was also observed at higher Nb content samples, e.g. Si/Nb-16. That could be because of strong interaction of Nb with the inner silica walls and dispersion of high surface Nb concentration. Similar results were observed in case of other transition metals such as V incorporated on mesoporous silica MCM-48 structured material and Nb-MCM-41 molecular sieves [35,38].

According to Zhang and Ying [35], the Nb incorporation into the framework occurs by two different steps. In the first step, the loosely bonded silica gel can access the heteroatom for incorporation at room temperature. In the second step, Nb is fully condensed into the framework silica under high temperature at hydrothermal conditions. However, in this present investigation we assume that the second mechanism occurred in the synthesis procedure.

Specific surface area, specific pore volume and pore diameter (BJH method) for calcined materials are presented in Table 1. N_2 isotherm of all calcined samples shows type IV isotherm (Fig. 2), which is typical for mesoporous materials. The isotherm shows well-defined stages and they coincide with those already reported

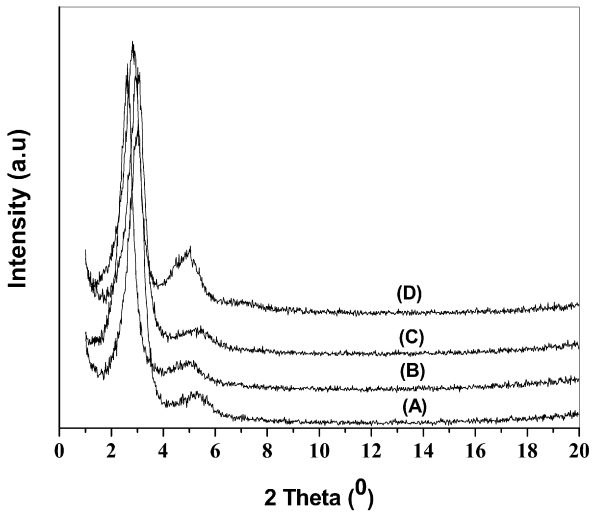

Fig. 1. XRD patterns of calcined mesoporous Nb-MCM-41 molecular sieves. (A) Si/Nb-16, (B) Si/Nb-32, (C) Si/Nb-64, (D) Si/Nb-128.

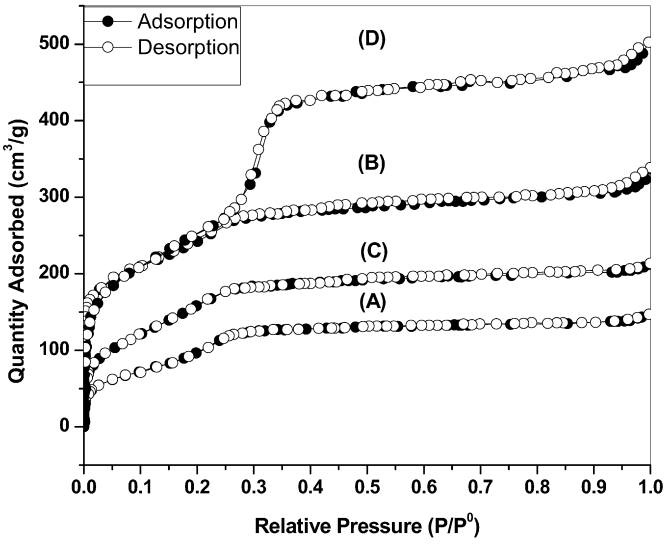

Fig. 2. N_2 adsorption and desorption isotherms of Nb-MCM-41 samples. (A) Si/Nb-16, (B) Si/Nb-32, (C) Si/Nb-64, (D) Si/Nb-128.

in literature [39]. However, the isotherm of sample Nb-MCM-41(Si/Nb-16) has already lost the characteristic mesoporous solid shape and its surface area decreased sharply to 417 m^2/g. The surface area of the catalysts decreased in the order Nb-MCM-41(Si/Nb-128) > Nb-MCM-41(Si/Nb-64) > Nb-MCM-41(Si/Nb-32) > Nb-MCM-41(Si/Nb-16). The decrease in the surface area and pore volume with increasing Nb loading can be attributed the formation of Nb_2O_5 species within the mesopores, which might at the same time block the pores of the mesopore structure. Thus, the incorporation of higher amounts of Nb disrupts the quality of Nb-MCM-41 material. Similarly, pore volumes decrease in the same order due to the presence of textural mesoporosity [40].

3.1.3. Diffuse reflectance UV–Vis spectra

Fig. 3 depicts the UV–Vis spectra of all calcined Nb-MCM-41 samples. The spectra of all calcined samples presented an intense band around 220 nm which can be assigned to Nb tetrahedrally coordinated to silica surface. The intense band at 260 nm in the spectra of samples with higher niobium loading (Nb-MCM-41 Si/Nb-32 and 16) is assigned to micro particles of Nb_2O_5 [41] which could be formed by leaching of niobium from the frame-

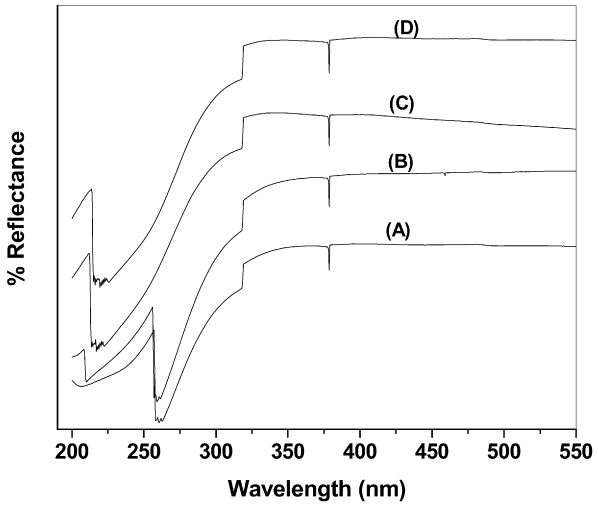

Fig. 3. UV–Vis spectra of Nb-MCM-41 molecular sieves. (A) Si/Nb-16, (B) Si/Nb-32, (C) Si/Nb-64, (D) Si/Nb-128.

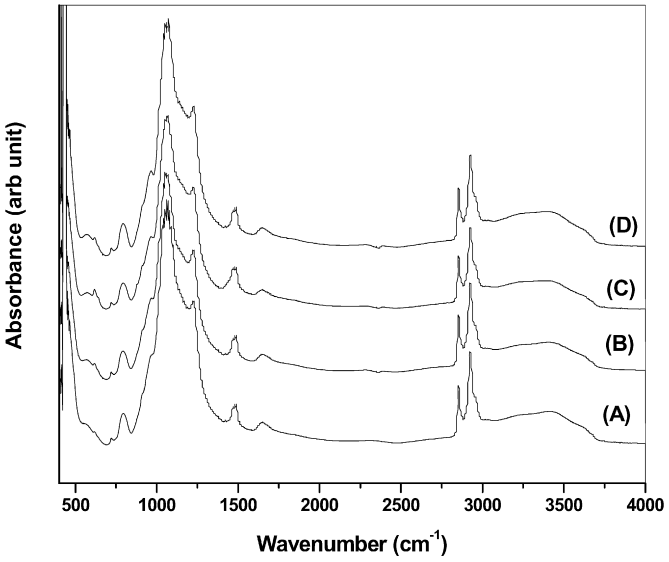

Fig. 4. FT-IR spectra of Nb-MCM-41 molecular sieves, as-synthesized samples. (A) Si/Nb-16, (B) Si/Nb-32, (C) Si/Nb-64, (D) Si/Nb-128.

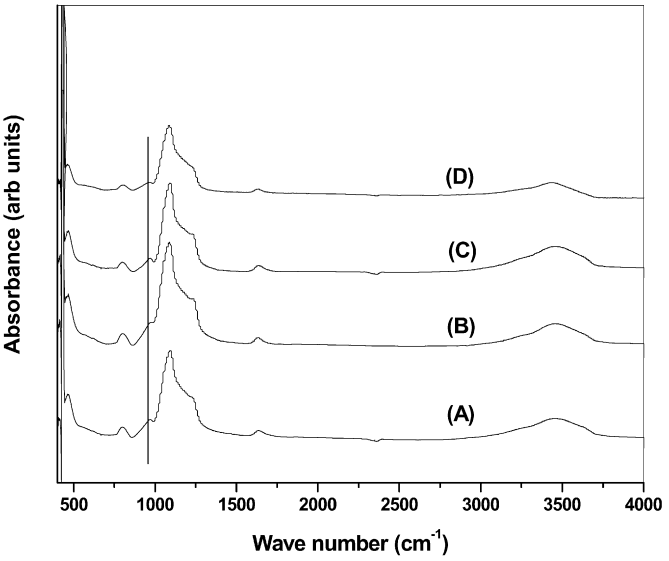

Fig. 5. FT-IR spectra of Nb-MCM-41 molecular sieves, calcined samples. (A) Si/Nb-16, (B) Si/Nb-32, (C) Si/Nb-64, (D) Si/Nb-128.

work. In these materials, niobium is coordinated to four oxygen atoms or interacting with an H_2O molecule, leading to distorted tetrahedral environment. Gallo et al. [37] described the mechanism of +5 oxidation state of niobium species incorporated in the framework of MCM-41 with octahedral geometry and change of the coordination of leaching niobium species during the calcination step. The intense band at 320 nm can be assigned to Nb octahedrally coordinated to the silica surface [42].

3.1.4. FT-IR spectroscopy

The IR-spectra of Nb-MCM-41 samples with different Si/Nb ratios of as-synthesized and calcined samples are shown in Figs. 4 and 5. In as-synthesized and calcined samples, the broad peak at 3500 cm^{-1} is attributed to the O–H stretching band of water, surface hydroxyl groups and bridged hydroxyl groups. The peaks in the spectra of as-synthesized samples below 3000 cm^{-1} are due to symmetric and asymmetric stretching of CH_2 group of the template. Their corresponding bending mode is observed at 1400 cm^{-1}. In the spectra of the calcined samples, the symmetric and asymmetric stretching modes of CH_2 groups of the template are absent, indicating complete removal of surfactant molecules from the matrix. These spectra resemble previously reported results [43,44]. The major peaks at 1220, 1080, 794 and 464 cm^{-1} are assigned to symmetric and asymmetric stretching of Si–O–Si vibrations. The characteristic band at ~970 cm^{-1} is attributed to the (Si–O–Nb) vibration [45]. However, in case of the Si-MCM-41 sample, the band at 960 cm^{-1} is attributed to the (Si–OH) vibration [46]. Indeed, the 970 cm^{-1} band cannot be taken as a characteristic band for the incorporation of Nb in the framework of Nb-MCM-41 samples. Nevertheless, a slight shift in the bands corresponding to the internal vibrations of TiO_4 units can be observed. Therefore, this shift may be taken as an indication of the transition metal incorporated in the framework. Similar results were observed for the incorporation of Ti and V in mesoporous Si sample [47].

3.1.5. Ammonia TPD

Ammonia TPD profiles of the catalysts with different Si/Nb ratios are shown in Fig. 6. It clearly shows a broad desorption signal in the region of 150–300 °C for all the samples. Results reveal that increasing the Nb concentration in the sample from (Si/Nb-128 to 16) shifted the desorption peak to higher temperature. It is indicative of an overall increase in concentration as well as strength of acid sites with increasing Nb concentration. Also, the acid strength increased from weak to medium with increasing Nb concentration. The probable sites responsible for enhancing the acid strength of Nb-MCM-41 samples with decreasing Si/Nb ratio are Si–O–Nb species. At higher Nb content, samples might have extra framework Nb species such as Nb_2O_5, which are responsible for increasing the acid strength [32]. At lower Nb content, the sample has shown weak acid sites that can be assigned to surface hydroxyl groups.

3.1.6. Pyridine FT-IR

The acidity of calcined materials was measured by pyridine FT-IR spectroscopy by using pyridine as a probe molecule. Desorption of pyridine occurred at 200 °C, and results are presented in Fig. 7. The main peaks can be assigned to the Lewis acid-bound (1450, 1575 and 1623 cm^{-1}), Brønsted acid-bound (1545 and 1640 cm^{-1}) and both Lewis and Brønsted acid-bound (1490 cm^{-1}) pyridine. It is also worth to note that at this desorption temperature Brønsted acid peaks are weak. Ziolek et al. [48] observed only the presence of Lewis acid sites at a desorption temperature of 150 °C. However,

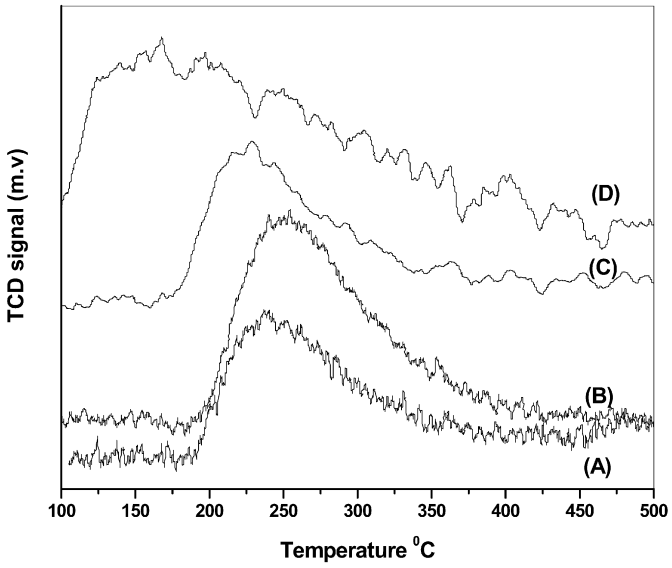

Fig. 6. Ammonia TPD of Nb-MCM-41 molecular sieves. (A) Si/Nb-16, (B) Si/Nb-32, (C) Si/Nb-64, (D) Si/Nb-128.

Table 2
^{29}Si NMR data of MCM-41 samples.

Sample	Si/Nb ratio	*I* (%)		
		Q^2 (−90 ppm)	Q^3 (−102 ppm)	Q^4 (−113 ppm)
Si-MCM-41		7	16	77
Nb-MCM-41 uncalcined	32	15	35	50
Nb-MCM-41	16	4	30	68
Nb-MCM-41	32	6	16	78
Nb-MCM-41	64	6	14	80
Nb-MCM-41	128	7	7	86

the present result indicates that Nb-MCM-41 molecular sieves have both Brønstead and Lewis acid sites.

3.1.7. ^{29}Si MAS NMR

The MAS NMR spectrum of calcined Si-MCM-41 and as-synthesized and calcined Nb-MCM-41(Si/Nb-32) samples (Fig. 8) shows three peaks at −113, −102 and −90 ppm corresponding to $Si(OSi)_4$ (Q^4), $Si(OSi)_3OH$ (Q^3), and $Si(OSi)_2(OH)_2$ (Q^2), respectively. Table 2 summarizes the relative integral intensities of Q^4, Q^3 and Q^2. In the present synthesis, we have observed a significant increase of Q^4 sites (50 to 78) at the expense of Q^3 and Q^2 during

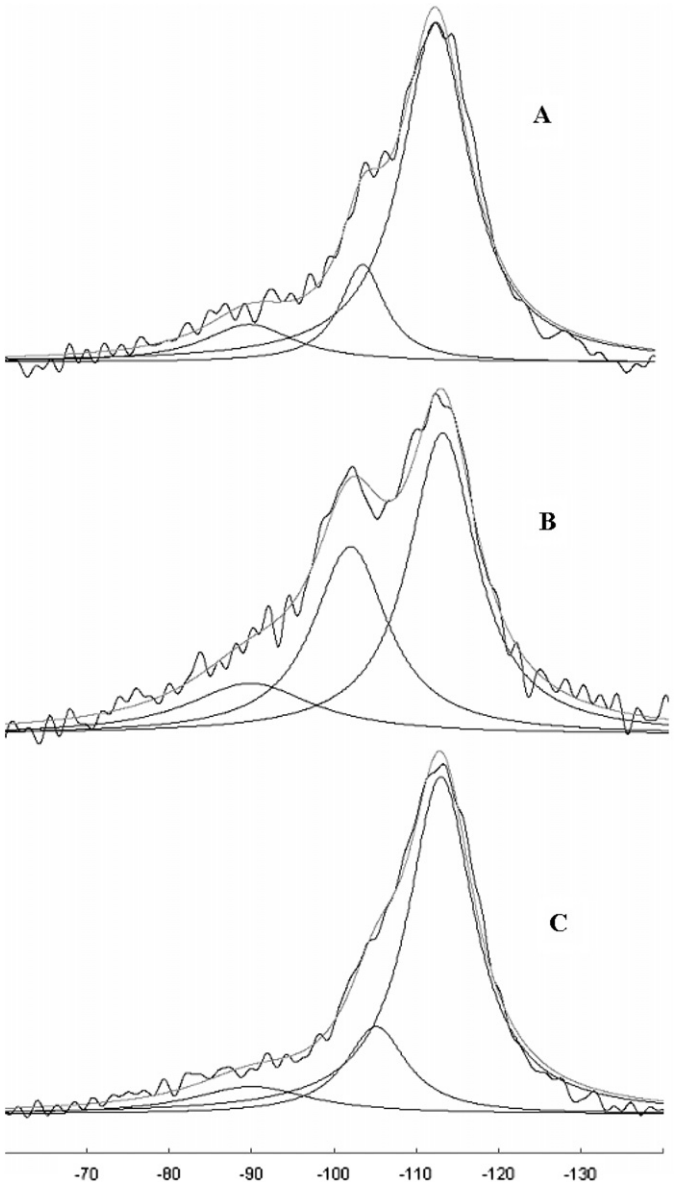

Fig. 8. ^{29}Si MAS NMR of (A) Si-MCM-41, (B) as-synthesized Nb-MCM-41(Si/Nb-32), (C) calcined Nb-MCM-41(Si/Nb-32).

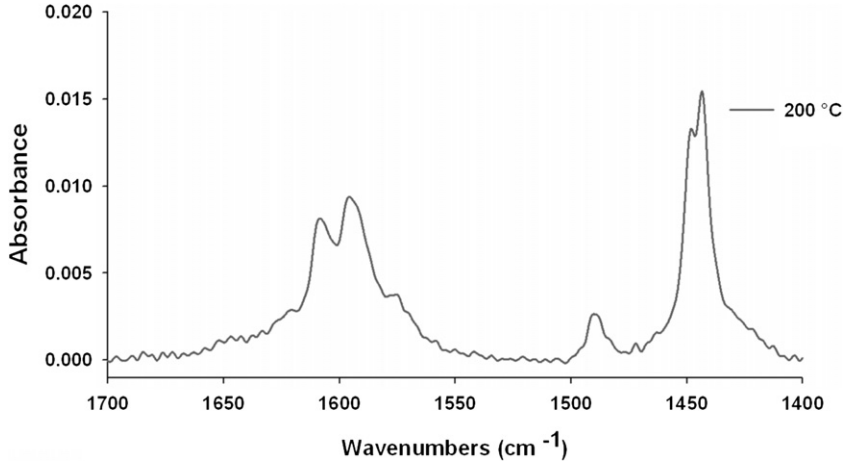

Fig. 7. Pyridine FT-IR of Nb-MCM-41 molecular sieves (Si/Nb-32).

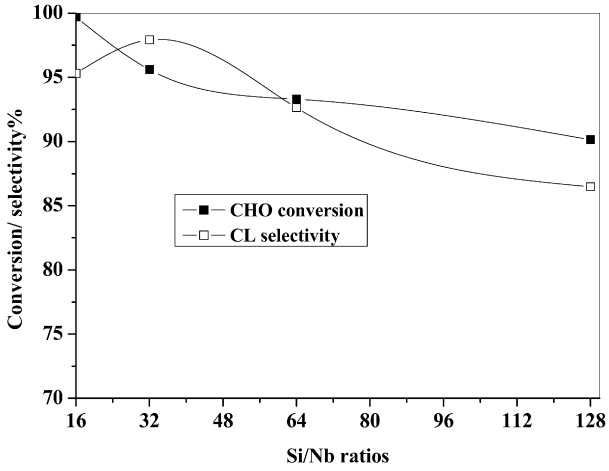

Fig. 9. Effect of Si/Nb ratios of different Nb-MCM-41 molecular sieves on the conversion and selectivity. Conditions: 300 °C, 0.1 bar, TOS = 4 h, WHSV = 0.3 h^{-1}, carrier gas = 2 l/h N_2, oxime:EtOH = 1:9 wt%.

the calcination. Thus, uncalcined samples exhibited higher fraction of incompletely cross-linked silica (Q^3 and Q^2). Therefore, calcination leads to higher level of silica condensation [47]. However, in case of the low niobium content samples (Si/Nb-64 and 128) the increase of Q^4 sides is noteworthy in contrast to Si-MCM-41. These results are attributed to the fact that niobium is incorporated into the silica framework and promotes the condensation of silanol sites. The same observation was made for other transition metals such as Ti and V incorporation in mesoporous silica framework [49,50]. Nevertheless, in contrast to the above-mentioned results, the Q^3 intensity also increased with increasing niobium content in the sample. It is possible that $Si(OSi)_3ONb$ is shifted to low field in comparison to $Si(OSi)_4$. The same behavior was observed in case of alumina-substituted zeolites [51]. According to this, it might be that $Si(OSi)_3ONb$ are appearing in same shift range as $Si(OSi)_3OH$. Indeed, we assume that the increase of intensity in the range of Q^3 sites is attributed to $Si(OSi)_3ONb$. This would also prove that Nb is incorporated into the framework.

3.2. Gas phase Beckmann rearrangement of CHO to CL

The gas phase Beckmann rearrangement of CHO to CL was carried out over Nb-MCM-41 (Si/Nb-16, 32, 64 and 128) catalysts. The effects of reaction temperature, solvent to substrate ratio, WHSV and time on stream were studied to optimize conversion and selectivity. In general, all catalysts exhibited very high conversions rates of CHO and very good selectivity to CL.

3.2.1. Influence of Si/Nb ratios

The effect of different Si/Nb ratios in the MCM-41 materials on catalytic performance is shown in Fig. 9. The CHO conversion and CL selectivity decreased with increasing Si/Nb ratios (i.e. with low amount of Nb content) of the sample. The CHO conversion rates and CL selectivities follow the order Nb-MCM-41(Si/Nb-16) > Nb-MCM-41(Si/Nb-32) > Nb-MCM-41(Si/Nb-64) > Nb-MCM-41(Si/Nb-128).

These catalytic activity results were correlated to the ammonia TPD profiles of the sample. The main reason for higher activity of samples with higher Nb content could be due to the medium acidic sites. Ammonia TPD profiles clearly indicated that with increasing Nb loading the strength of acid sites increased from weak to medium. Thus, these results indicate that the CHO conversion is strongly dependent on the amount and strength of the acid sites. The spectroscopic analysis of DR–UV–Vis results suggested that, with increasing Nb loading, extra framework Nb_2O_5 species appeared in the samples. It could be that these extra framework Nb_2O_5 species are also responsible for such strong activation of this reaction. However, many researchers have reported the catalytic activity relationship with acidity of the catalysts. Kob et al. assumed that strong acid sites were more favorable for the reaction than the weak acid sites [6]. In contrast, Hölderich et al. reported that weakly acidic vicinal silanol groups and nest silanol sites are the active sites for the selective formation of CL [2,3,16,23,52]. These findings are confirmed by recent solid-state NMR studies [53,54]. In addition, Beckmann rearrangement proceeds on Brønsted and Lewis acid sites. Pyridine FT-IR spectra results of Nb-MCM-41(Si/Nb-32) catalyst have shown presence of both Brønsted and Lewis acid sites with distribution of weak to medium acid sites. All Nb-MCM-41 catalysts with different Si/Nb ratios display very good conversion rates of almost 100% with high selectivities for CL of >95%.

3.2.2. Influence of reaction temperature

The product distribution and catalytic activity were strongly dependent upon the reaction temperature. The influence of reaction temperature over Nb-MCM-41(Si/Nb-32) catalyst was studied at 250, 300, and 350 °C, and the results are depicted in Fig. 10. The reactant feed weight ratio (CHO:ethanol) was kept at 1:9 and WHSV was 0.3 h^{-1}. CHO conversion and CL selectivity increased with increasing reaction temperature from 250 to 300 °C. CL was formed more selectively than the other compounds at higher temperatures. At lower reaction temperatures, cyclohexanone was the main by-product that is formed by decomposition of CHO. Desorption is not fast enough at lower temperature. Therefore, the intrinsic residence time is high and causes decomposition of CHO. At 300–325 °C temperature, the CHO conversion and CL selectivities are higher (98.5 and 95.5%) due to the lower oligomerization of CHO. However, at higher temperature (350 °C) the CL selectivity (87.7%) decreased, because the ring opening reaction of CL to the hexenenitrile occurs. However, constant CHO conversion (98.7%) is still observed. These results indicate that at 300–325 °C the main reaction was Beckmann rearrangement to CL. Also, thermodynamic data clearly illustrated that a slight increase of $\Delta_r G°$ with temperature may indicate that lower temperatures are favorable for Beckmann rearrangement reaction. At high temperature the side-product formation in thermodynamic equilibrium would be strongly favored [55]. Nevertheless, 300–325 °C is a somewhat higher temperature than in the case of deboronated pentasil type catalyst, where optimum reaction temperature was about 280–300 °C [3,18,52]. Recently, Conesa et al. [56,57] observed that 425–450 °C is optimum reaction temperature for obtaining high CL selectivities in gas phase Beckmann rearrangement in presence of mesoporous silicaalumino phosphate and Al-B-MCM-41 catalysts. Nevertheless, in our present investigations almost 100% conversion of CHO and above 95% selectivity for CL were already achieved at around 300 °C.

3.2.3. Influence of weight hourly space velocity (WHSV)

The influence of WHSV of the feed on conversion and selectivity to the products over Nb-MCM-41(Si/Nb-32) catalyst is illustrated in Fig. 11. While the catalyst weight is kept at 2 g, the contact time was varied by changing the feed rate so that WHSV = 0.2–4 h^{-1}. A continuous decrease of CHO conversion from 100 to 30% is observed with increasing the WHSV of the feed from 0.2 to 0.4 h^{-1}. The maximum yield of CL with 95.9% is observed at a WHSV of 0.3 $g_{reactant}\, g_{cat}^{-1}\, h^{-1}$.

In the present investigation, when the WHSV was increased from 0.2 to 2.5 h^{-1}, the selectivity to 5-hexenenitrile and other selectivity increased, however, we could not observe significant changes in the selectivity to CL and other products by variation of WHSV.

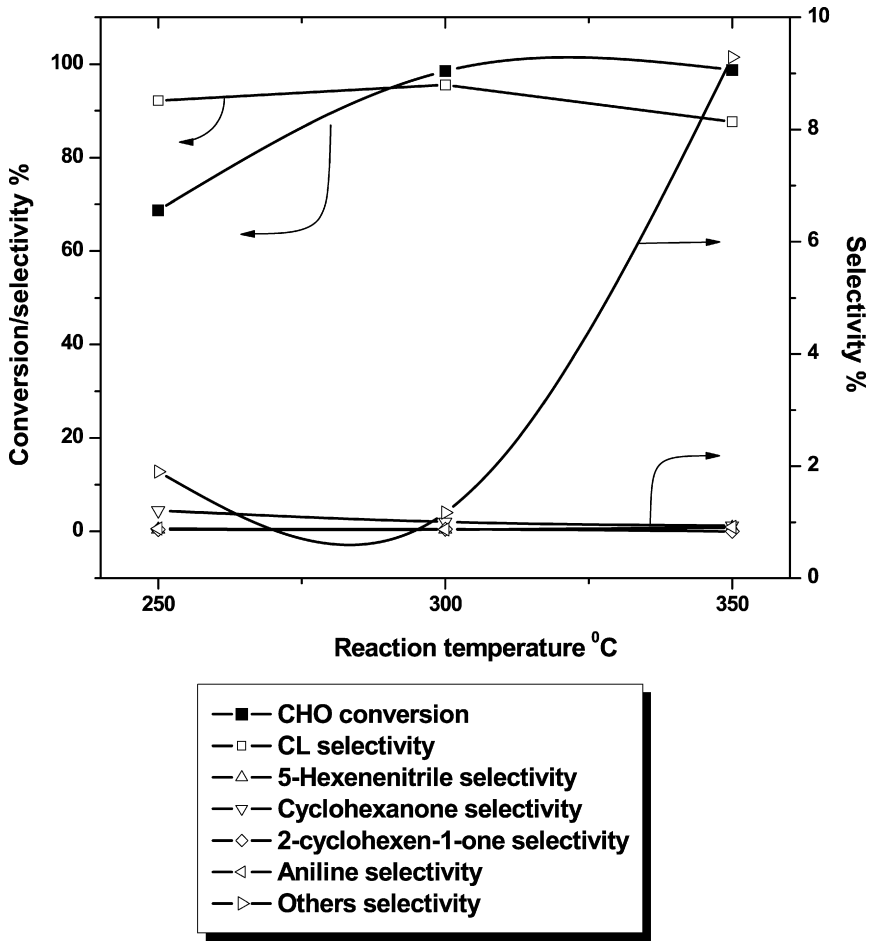

Fig. 10. Effect of temperature on the conversion and selectivity over Nb-MCM-41(Si/Nb-32) catalyst. Conditions: 0.1 bar, time = 4 h, WHSV = 0.3 h^{-1}, carrier gas = 2 l/h N_2, CHO:EtOH = 1:9 wt%.

Table 3
Effect of feed ratios over Nb-MCM-41(Si/Nb-32).

Feed ratios (ethanol:CHO)	CHO conversion (%)		CL selectivity (%)	
	After 2 h	After 10 h	After 2 h	After 10 h
1:9	94.5	92.2	96.6	97.9
1:6	71.3	57.7	96.0	99.3
1:3	73.0	56.6	98.3	99.3

3.2.4. Influence of feed ratio

The influence of feed ratios in the reaction was studied with 1:3, 1:6 and 1:9 CHO:ethanol weight ratio in the presence of Nb-MCM-41(Si/Nb-32) catalyst. The reactions were carried out at 300 °C and WHSV = 0.3 h^{-1} for 10 h. The results are presented in Table 3. The higher the dilution feed such as CHO:ethanol = 1:9 the higher the conversion of CHO. At a low dilution, i.e. feed ratios 1:6 and 1:3, the conversion decreased with time on stream. The CL selectivity was constant at all chosen feed ratios. The higher catalytic activity in presence of high concentration of ethanol in the feed may be due to the enhancement of CL desorption from the catalyst active centers.

3.2.5. Time on stream study

The reaction was carried out for 100 h over Nb-MCM-41(Si/Nb-128) catalyst to study the deactivation of the catalyst. The results (Fig. 12) revealed that the catalyst shows very good activity in both CHO conversion and CL selectivity for 40 h. After that, the CHO conversion began to decrease. The conversion declined to 40% after 100 h of time on stream. However, the selectivity for CL of 97% was found almost constant during 100 h time on stream. The catalyst deactivation proceeds most probably via poisoning of the active sites. These results are in good agreement to those previously reported in case of H-MCM-22 catalyst [58]. The catalytic stability can be divided into two periods: Period I—up to 40 h—exhibiting stable conversion, and period II—up to 100 h—with rapid ageing of the catalyst. It is well known that catalyst deactivation in the Beckmann rearrangement of CHO is caused by formation of coke and oligomers on the catalyst surface. Moreover, it was observed that when more acid sites of MFI zeolite are present for this reaction, ring-opening reaction occurred and more oligomer precursors were formed on the catalyst surface [59]. Surprisingly, in our present study we did not observe significant increase of the selectivity to ring opening reaction products such as hexenenitrile compounds.

Furthermore, to elucidate the type of coke formed on the catalyst surface, after 100 h, spent Nb-MCM-41(Si/Nb-128) catalyst was measured with XPS analysis. The XPS data for spent catalyst showed (Table 4) a C 1s signal at binding energies of 284.8–285.5 eV, which is an indication that presence of aliphatic carbon on the catalyst surface [60,61] and not for carbon of aromatic or SP^2-character [62,63]. In addition, the XPS depth profile shows that nitrogen had penetrated into the material as well. The N 1s signal appeared at a binding energy of about 399–400 eV, which is corresponding to aminofunctional and ammonium-like species present on the surface [64]. This might indicate that hexane nitrile compounds are formed and subsequently oligomerized or polymerized, resulting in the blockage of the pores. Similar kind of results was

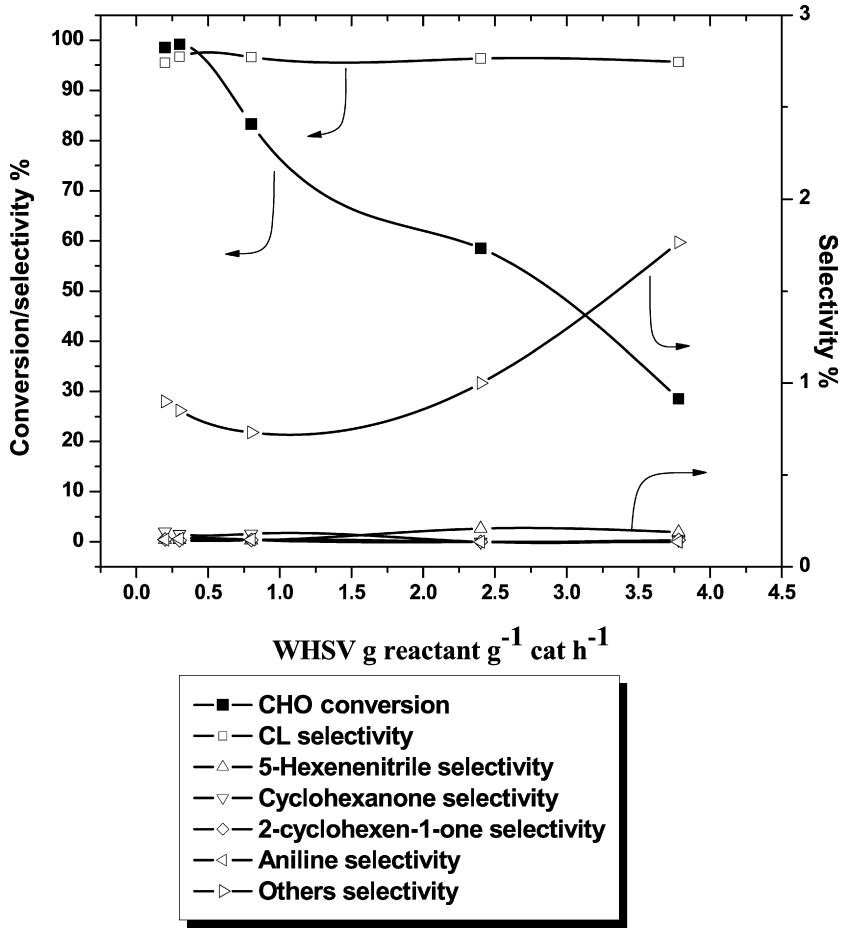

Fig. 11. Effect of WHSV on conversion and selectivity over Nb-MCM-41(Si/Nb-32) catalyst. Conditions: 300 °C, 0.1 bar, TOS = 4 h, carrier gas = 2 l/h N_2, CHO:EtOH = 1:9 wt%.

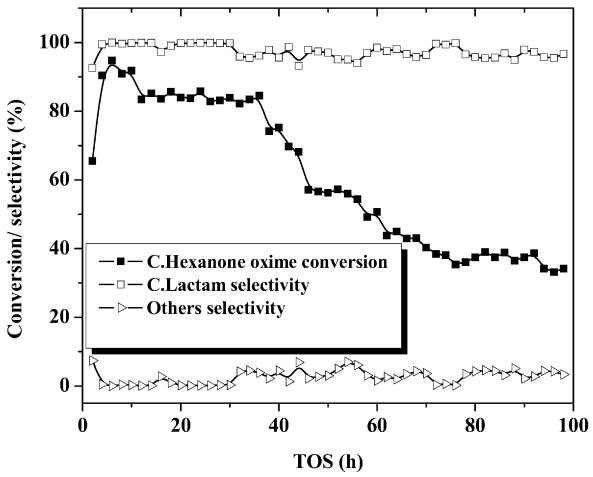

Fig. 12. Time on stream study of the Nb-MCM-41(Si/Nb-128). Conditions: 300 °C, pressure = 0.1 bar, WHSV = 0.3 h^{-1}, carrier gas = 2 l/h N_2, CHO:EtOH = 1:9 wt%.

observed in case of B-MFI catalysts and it was intensively investigated in both fresh and deactivated catalysts by secondary ion mass spectroscopy (SIMS) and X-ray photoelectron spectroscopy (XPS) [59].

In order to reveal the reason for the deactivation of Nb-MCM-41(Si/Nb-128) catalyst in the gas phase Beckmann rearrangement of CHO to CL, the catalyst was analyzed by N_2 adsorption method after 100 h TOS. Table 5 shows the decrease of pore diameter and surface area of used catalyst in comparison with the fresh catalyst.

Table 4
Results of the XPS data of Nb-MCM-41(Si/Nb-128) after 100 h.

Surface concentration	Given in atomic percent	Binding energy in eV
C 1s	21.21	285.5
O 1s	55.19	533
N 1s	3.32	399.5
Si 2p	20.28	104.5
Nb 3d	Traces	–

Table 5
Surface area and pore diameter for Nb-MCM-41(Si/Nb-128) before and after reaction.

Catalyst	Surface area (m^2/g)	Pore diameter (Å)
Nb-MCM-41(Si/Nb-128) fresh	929	29.27
Nb-MCM-41(Si/Nb-128) after 100 h TOS	414	20.8

This behavior is attributed to catalyst active sites being uniformly blocked by by-products and consecutive reaction products like nitriles and polymeric species.

3.2.6. Catalyst regeneration study under air or under non-oxidative gas

Sato et al. examined the regeneration of non-zeolitic catalyst such as B_2O_3/Al_2O_3 catalyst by burning off the coke in air at 500 °C for 3 h and found that while CHO conversion was completely recovered, CL selectivity was poorer [65]. On the other hand, Dahlhoff et al. developed a regeneration method for deactivated B-MFI catalysts in a fluidized bed reactor [66,67]. Hölderich and co-workers investigated the long-term regeneration stability

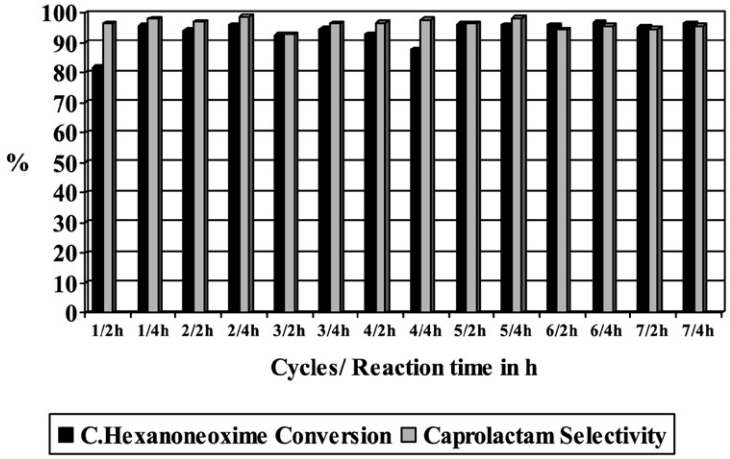

Fig. 13. Catalyst recycle studies under air with Nb-MCM-41(Si/Nb-32). Conditions: 300 °C, 0.1 bar, WHSV = 0.3 h^{-1}, carrier gas = 2 l/h N_2, oxime:EtOH = 1:9 wt%, regeneration conditions under air at 500 °C for 4 h.

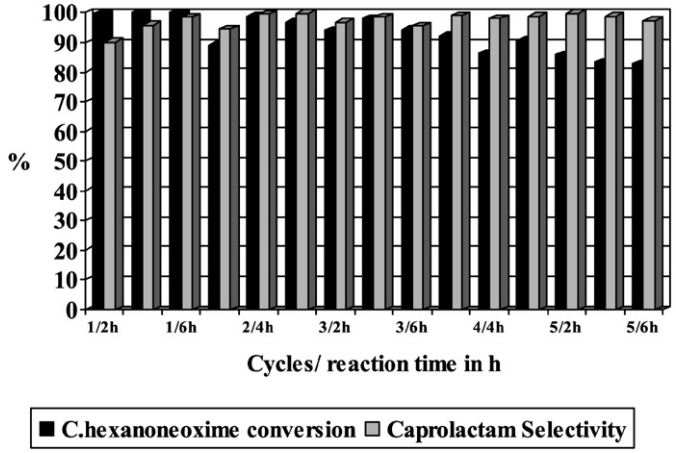

Fig. 14. Catalyst recycle studies under N_2 with Nb-MCM-41(Si/Nb-32). Conditions: 300 °C, 0.1 bar, WHSV = 0.3 h^{-1}, carrier gas = 2 l/h N_2, oxime:EtOH = 1:9 wt%, regeneration conditions under N_2 at 500 °C for 4 h.

of specially modified B-MFI catalysts as well as MCM-22 catalysts over 40 days. The catalyst was regenerated at 500 °C for 16 h under air after 6 h reaction time [68,69]. Also, they found that the regeneration could be carried out in a non-oxidative atmosphere such as N_2 [66].

The present regeneration study was conducted on a deactivated Nb-MCM-41(Si/Nb-32) catalyst under air or non-oxidative gas such as N_2 for five or more cycles. The results based on CHO conversion and CL selectivity are illustrated in Figs. 13 and 14. In both the cases the catalyst could be regenerated five or even more cycles without any considerable activity loss. The regeneration study under air has shown almost constant activity for seven cycles. When the catalyst was regenerated in the presence of air at 500 °C for 4 h, the original activity was completely recovered.

In contrast, when the regeneration was performed under N_2 gas at 500 °C for 4 h, CHO conversion started to decrease after five cycles from 100 to 85%, the CL selectivity, however, increased to almost 100% by the end of five cycles.

Based on the above results it is concluded that the pore blockage by coke/oligomers is the main reason for deactivation of the catalyst. These oligomers, which are formed by ring opening reaction, can be desorbed or washed off with nitrogen or other oxidative gases as we found before [66]. Moreover, the regeneration studies under air and N_2 concluded that the deactivation is reversible.

In addition, we observed that catalyst color changed to black after the reaction, suggesting that the catalyst is at least partly covered with coke. Consequently, the amount of coke formation on the spent catalysts was measured by TG and DTA analysis. After five regeneration cycles of the catalyst under nitrogen, catalyst was characterized by TG and DTA analysis. It was observed that after TG analysis the white color of the catalyst was restored as a result of coke combustion. The relationship between amount of coke formed on the catalyst surface and combustion temperature is depicted in Fig. 15.

TG and DTA analysis results of spent catalyst revealed that all the coke from the catalysts surface can be removed at 300–500 °C. The combustion of the coke caused a sudden decrease of TGA signal at 300 to 500 °C. The weight loss is approximately 35% observed. DTA analysis results of spent catalyst show a strong exothermic peak around 450 °C and shoulder peak at 300 °C, which are attributed to combustion and removal of coke from the catalyst.

3.2.7. Reaction results by following Design Expert

In order to determine the optimum reaction conditions, reactions are carried out using response surface design for Nb-MCM-41(Si/Nb-32) catalyst. From above studies it was found that the reaction temperature and WHSV play the major role in conversions and selectivities. Indeed, the reactions are carried out by changing these two factors, in contrast the other reaction conditions such as feed ratio, reduced pressure and carrier gas flow are maintained constant.

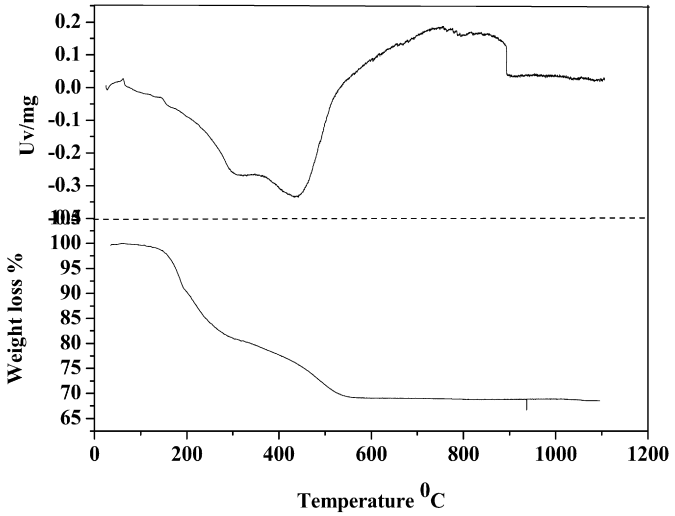

Fig. 15. TG and DTA analysis of Nb-MCM-41(Si/Nb-32) catalyst after five cycle regeneration under N_2 gas.

Design-Expert model results are shown in Figs. 16–18. Results clearly illuminate that at high temperatures of around 300–325 °C, and at high WHSV of around 0.4 h^{-1} values, 100% CHO conversion can be achieved. At lower temperature 250 °C, the conversion reached maximum about 30%. The CL selectivity is increased with reaction temperature from 250 to 300 °C and WHSV value from 0.2 to 0.4 h^{-1}. With further increase the reaction temperature from 300 to 350 °C and WHSV values from 0.4 to 1 h^{-1} the CL selectivity is decreased. At the same time the selectivity for other by-products started to increase. As a result we can conclude that 300 °C and a WHSV = 0.4 h^{-1} are suitable to achieve 100% CHO conversion and more than 95% CL selectivity.

Table 6
Design-Expert model solutions.

S. No.	Temperature (°C)	WHSV (h^{-1})	C. oxime conversion (%)	C. lactam selectivity (%)	Others selectivity (%)	Durability
1	297.47	0.27	96.62	95	5	1
2	326.93	0.49	99.99	95	5	1
3	304.99	0.30	98.35	95	5	1
4	316.59	0.39	99.61	95	5	1
5	273.99	0.26	83.15	95	5	1
6	268.73	0.28	77.67	95	5	1
7	325.84	0.48	99.96	95	5	1
8	276.98	0.25	85.77	95	5	1
9	328.09	0.51	100	95	5	0.99

To obtain a better reproducibility and standard conditions for the reaction, the Design-Expert model has given 9 predicted reaction conditions with durability of one. Table 6 presented the predicted values of conversion and selectivity with different temperature and WHSV values.

For checking the durability, reactions were carried out by according to the reaction conditions predicted from solutions of Desing-Expert model (Table 6: S. Nos. 3, 5 and 7). Reaction results were summarized in Table 7. These results clearly illustrate that experimental results are nearly same as predicted values of design expert model.

4. Conclusions

From this work the following conclusions are drawn:

- Nb-MCM-41 molecular sieves with different Si/Nb ratios have been synthesized and characterized by various spectroscopic techniques. These analytical results provided strong evidence that Nb has been incorporated into the mesoporous silica

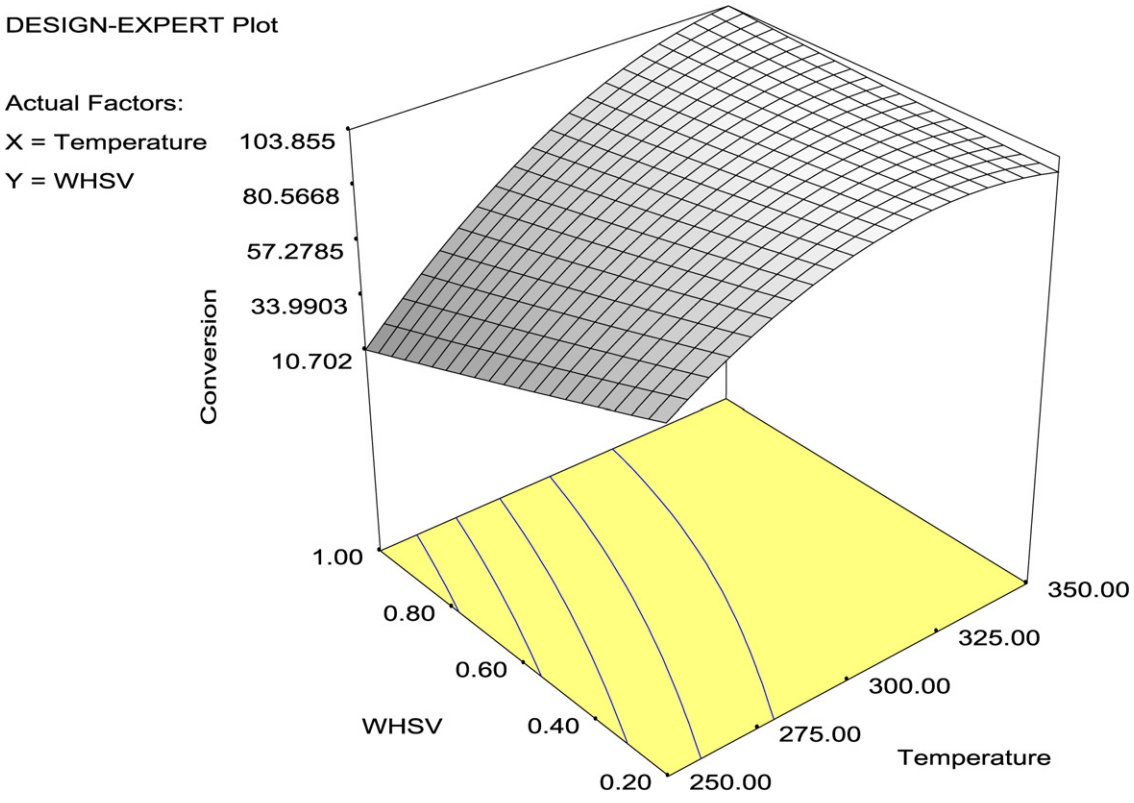

Fig. 16. CHO conversion over Nb-MCM-41(Si/Nb-32). Conditions: 0.1 bar, carrier gas = 2 l/h N_2, CHO:EtOH = 1:9 wt%, TOS = 4 h.

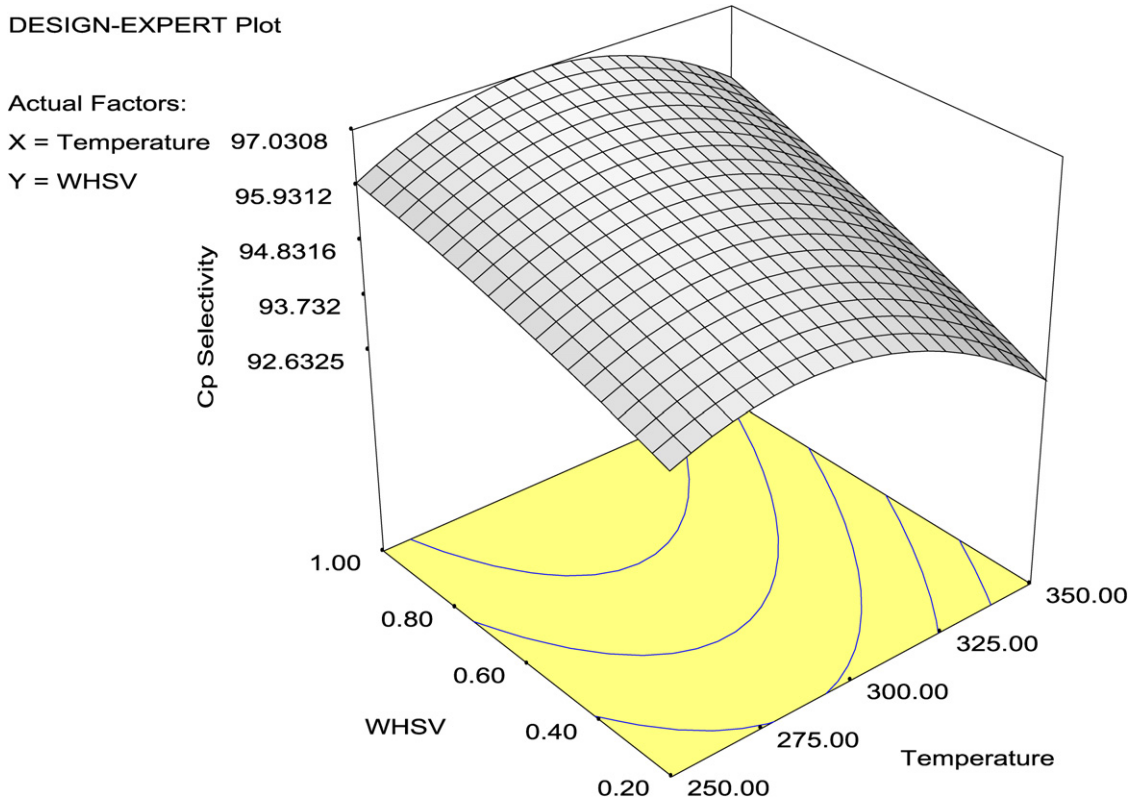

Fig. 17. CL selectivity over Nb-MCM-41(Si/Nb-32). Conditions: 0.1 bar, carrier gas = 2 l/h N_2, CHO:EtOH = 1:9 wt%, TOS = 4 h.

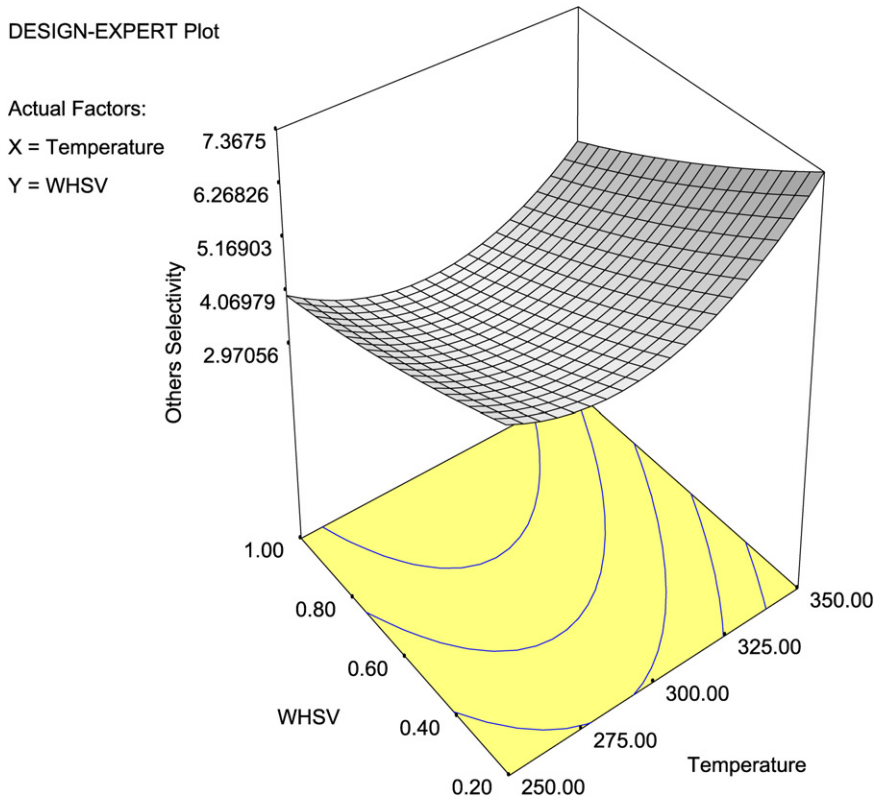

Fig. 18. Selectivity of others over Nb-MCM-41(Si/Nb-32). Conditions: 0.1 bar, carrier gas = 2 l/h N_2, CHO:EtOH = 1:9 wt%, TOS = 4 h.

framework and all samples have well-ordered mesoporous structure with uniform pore size.

- N_2 sorption studies revealed that with increasing Nb content, partial loss of mesoporous structure occurred.
- DR–UV–Vis spectroscopy results revealed that Nb-MCM-41 molecular sieves contain two types of niobium species, one is tetrahedrally coordinated Nb species in framework, while the other is polymerized hydrated Nb_2O_5 species on the

Table 7
Comparison of reaction results with predicted results.

	Temperature (°C)	WHSV (h^{-1})	C. oxime conversion (%)	C. lactam selectivity (%)	Others selectivity (%)
Predicted	305	0.3	98.4	95	5
Achieved results	300	0.3	99.2	96.7	3.3
Predicted	326	0.48	100	95	5
Achieved results	326	0.5	96.1	97.5	2.6
Predicted	274	0.26	83.2	95	5
Achieved results	274	0.25	82.3	91.4	8.6

outer surface, which are present in higher Nb content samples.

- ^{29}Si MAS NMR, and FT-IR spectroscopic results indicated the presence of Si–O–Nb linkage, confirming the Nb incorporation into Si framework.
- Ammonia TPD results revealed that with increasing Nb loading the acid sites moved from weak to medium acid strength. Also, pyridine FT-IR spectroscopic results confirmed that Nb-MCM-41 molecular sieves have both Brønsted and Lewis acid sites.
- Rearrangement of CHO carried out on Nb-MCM-41 with different Si/Nb ratios showed that catalysts are highly active for highest Si/Nb ratios. Thus, the catalytic activity mainly depends on the acidity of the catalyst and the acidity of the samples is strongly dependent upon the effect of niobium content in the sample.
- Temperature and WHSV studies suggested that 300–325 °C, and about 0.4 h^{-1} are optimum reaction conditions for this reaction.
- The catalyst deactivation when using different feed ratios follows the order of CHO:ethanol weight ratios 1:3 > 1:6 > 1:9.
- Time on stream studies indicate that the catalyst maintained constant activity for up to 40 h, afterwards, the conversion started to decrease. Nevertheless, constant CL selectivity was observed during 100 h time on stream. This indicates that catalyst deactivates due to the poisoning of catalyst active sites either by coke or by oligomers. In addition, a decrease of surface area and pore diameter was observed after 100 h reaction time.
- The regeneration study revealed that catalysts can be regenerated in oxidative or even a non-oxidative gas as N_2, and reaction can be carried out without significant loss of catalytic activity.
- The TG and DTA analysis of spent catalyst regenerated under N_2 showed around 35 wt% loss observed after the 5th cycle. All coke could be removed from the catalyst surface by heating the samples at 500 °C for 4 h under N_2 or air.
- Design-Expert model results revealed that temperature of 325 °C and WHSV of 0.4 h^{-1} are optimum reaction conditions for obtaining 100% CHO conversion and above 95% CL selectivity.

Acknowledgments

The authors are grateful to Sumitomo Chemical Co., Ltd., Niihama, Japan in particular of Dr. C. Stoecker, Dr. M. Kitamura and his co-workers for the constant interest in our studies and fruitful discussions. Also, we express sincere thanks to Dr. M. Valkenberg, Mr. Karl Joseph Vaesen, Mrs. Elke Biener, Mrs. R. Hinze all of our department TCHK, RWTH, Mr. H. Windgassen, IHT, RWTH and Mr. R. Koufmann, DWI, RWTH Aachen for various characterization studies.

Supplementary material

The online version of this article contains additional supplementary material.

Please visit DOI: 10.1016/j.jcat.2008.08.019.

References

[1] Ullmanns Encyclopedia of Industrial Chemistry, sixth ed., 1998, electronic release.
[2] W.F. Hölderich, J. Röseler, G. Heitmann, A.T. Liebens, Catal. Today 37 (1997) 353.
[3] G. Dahlhoff, J.P.M. Niederer, W.F. Hölderich, Catal. Rev. Sci. Eng. 43 (2001) 381.
[4] A. Costa, P.M. Deyá, J.V. Sinisterra, J.M. Marinas, Can. J. Chem. 58 (1980) 1266.
[5] G. Cimino, P. Vitarelli, G. Alibrandi, C. Caristi, S. Galvagno, React. Kinet. Catal. Lett. 21 (1982) 467.
[6] N. Kob, R.S. Drago, Catal. Lett. 49 (1997) 229.
[7] T. Ushikubo, K. Wada, J. Catal. 148 (1994) 138.
[8] H. Sharghi, M.H. Sarvari, J. Chem. Res. 3 (2003) 176.
[9] S. Sato, K. Urabe, Y. Izumi, J. Catal. 102 (1986) 99.
[10] P.S. Landis, P.B. Venuto, J. Catal. 6 (1966) 245.
[11] H. Ichihashi, M. Kitamura, Catal. Today 73 (2002) 23.
[12] H. Ichihashi, H. Sato, Appl. Catal. A Gen. 221 (2001) 359.
[13] Y. Izumi, H. Ichihashi, Y. Shimazu, M. Kitamura, H. Sato, Bull. Chem. Soc. Jpn. 80 (2007) 1280.
[14] A. Thangaraj, S. Sivasanker, P. Ratnasamy, J. Catal. 137 (1992) 252.
[15] P.S. Singh, R. Bandyopadhyay, S.G. Hegde, B.S. Rao, Appl. Catal. A Gen. 136 (1996) 249.
[16] G.P. Heitmann, G. Dahlhoff, W.F. Hölderich, Appl. Catal. A Gen. 185 (1999) 99.
[17] C. Ngamcharussrivichai, P. Wu, T. Tatsumi, J. Catal. 235 (2005) 139.
[18] G.P. Heitmann, G. Dahlhoff, W.F. Hölderich, J. Catal. 186 (1999) 12.
[19] T. Yashima, N. Oka, T. Komatsu, Catal. Today 38 (1997) 249.
[20] W.-C. Li, A.-H. Lu, R. Palkovits, W. Schmidt, B. Spliethoff, F. Schüth, J. Am. Chem. Soc. 127 (2005) 12595.
[21] K. Chaudhari, R. Bal, A.J. Chandwadkar, S. Sivasanker, J. Mol. Catal. A Chem. 177 (2002) 247.
[22] J. Röseler, G. Heitmann, W.F. Hölderich, Proceedings of the 11th Int. Zeolite Conf., Aug. 12–17, 1996, Seoul, Korea, Stud. Surf. Sci. Catal. 105 (1997) 1173.
[23] W.F. Hölderich, G. Heitmann, Catal. Today 38 (1997) 227.
[24] H. Ichihashi, M. Kitamura, H. Kajlkurl, E. Tasaka, US patent 5,354,859 (1994) to Sumitomo Chemical Co. Ltd.
[25] M. Kitamura, H. Ichihashi, H. Tojima, US patent 5,403,801 (1995) to Sumitomo Chemical Co. Ltd.
[26] M. Kitamura, Y. Shimazu, M. Yako, US patent 6,265,574 (2001) to Sumitomo Chemical Co. Ltd.
[27] M. Ziolek, I. Nowak, Zeolites 18 (1997) 356.
[28] B. Kilos, M. Aouine, I. Nowak, M. Ziolek, J.C. Volta, J. Catal. 224 (2004) 314.
[29] J.M.R. Gallo, H.O. Pastore, U. Schuchardt, J. Catal. 243 (2006) 57.
[30] L. Cedeño, D. Hernandez, T. Klimova, J. Ramirez, Appl. Catal. A Gen. 241 (2003) 39.
[31] I. Nowak, M. Ziolek, Chem. Rev. 99 (1999) 3603.
[32] H. Jung, K.-D. Jung, O.-S. Joo, S.J. Kim, Solid State Phenom. 124–126 (2007) 1761.
[33] S. Vetrivel, A. Pandurangan, Catal. Lett. 99 (2005) 141.
[34] E. Scheffier, Statistische Versuchsplanung, DVG, Stuttgart, 1997.
[35] L. Zhang, J.Y. Ying, AIChE J. 43 (1997) 2793.
[36] P. Selvam, S.K. Bhatia, C.G. Sonwane, Ind. Eng. Chem. Res. 40 (2001) 3237.
[37] J.M.R. Gallo, I.S. Paulino, U. Schuchardt, Appl. Catal. A Gen. 266 (2004) 223.
[38] M. Morey, A. Davidson, H. Eckert, G. Stucky, Chem. Mater. 8 (1996) 486.
[39] S.J. Greggand, K.S.W. Sing, Adsorption, Surface Area and Porosity, second ed., Academic Press, New York, 1982.
[40] T.R. Pauly, Y. Liu, T.J. Pinnavaia, S.J.L. Billinge, T.P. Rieker, J. Am. Chem. Soc. 121 (1999) 8835.
[41] A.M. Prakash, L. Kevan, J. Am. Chem. Soc. 120 (1998) 13148.
[42] M. Nishimura, K. Asakura, Y. Iwasawa, J. Chem. Soc. Chem. Commun. 22 (1986) 1660.
[43] S. Biz, M.L. Occelli, Catal. Rev. Sci. Eng. 40 (1998) 329.
[44] C.Y. Chen, H.X. Li, M.E. Davis, Microporous Mater. 2 (1993) 17.
[45] M. Selvaraj, B.H. Kim, T.G. Lee, Chem. Lett. 34 (2005) 1290.
[46] M.A. Camblor, A. Corma, J.P. Pariente, J. Chem. Soc. Chem. Commun. 6 (1993) 557.
[47] S.C. Laha, R. Kumar, Microporous Mesoporous Mater. 53 (2002) 163.
[48] M. Ziolek, I. Nowak, J.C. Lavalley, Catal. Lett. 45 (1997) 259.
[49] S. Shylesh, A.P. Singh, J. Catal. 228 (2004) 333.
[50] W. Zhang, J. Wang, P.T. Tanev, T.J. Pinnavaia, J. Chem. Soc. Chem. Commun. (1996) 979.
[51] A.T. Bell, A. Pines, NMR Techniques in Catalysis, Marcel Dekker, Inc., New York, 1994, p. 19.
[52] G.P. Heitmann, G. Dahlhoff, J.P.M. Niederer, W.F. Hölderich, J. Catal. 194 (2000) 122.

[53] V.R.R. Marthala, Y. Jiang, J. Huang, W. Wang, R. Gläser, M. Hunger, J. Am. Chem. Soc. 128 (2006) 14812.
[54] V.R. Reddy Marthala, S. Rabl, J. Huang, S.A.S. Rezai, B. Thomas, M. Hunger, J. Catal. (2008) 1.
[55] G.P. Heitmann, G. Dahlhoff, W.F. Hölderich, Chem. Eng. Technol. 22 (1999) 9.
[56] T.D. Conesa, R. Mokaya, Z. Yang, R. Luque, J.M. Campelo, A.A. Romero, J. Catal. (2007) 1.
[57] T.D. Conesa, J.M. Campelo, D. Luna, J.M. Marinas, A.A. Romero, Appl. Catal. B Environ. 70 (2007) 567.
[58] C.C. Tsai, C.Y. Zhong, I. Wang, S.B. Liu, W.H. Chen, T.C. Tsai, Appl. Catal. A Gen. 267 (2004) 87.
[59] P. Albers, K. Seibold, T. Haas, G. Prescher, W.F. Hölderich, J. Catal. 176 (1998) 561.
[60] C.D. Wagner, W.M. Riggs, L.E. Davis, J.F. Moulder, G.E. Muilenberg, Hand Book of X-Ray Photoelectron Spectroscopy, Perkin Elmer, Physical Electronics Division, Eden Prairie, MI, 1978.
[61] G. Barth, R. Lindner, C. Bryson, Surf. Interface Anal. 11 (1988) 307.
[62] E. Desimoni, G.I. Casella, A. Morone, A.M. Salvi, Surf. Interface Anal. 15 (1990) 627.
[63] H. Darmstadt, C. Roy, S. Kaliaguine, Carbon 32 (1994) 32.
[64] P.W. Albers, H. Klein, E.S. Lox, K. Seibold, G. Prescher, S.F. Parker, Phys. Chem. Chem. Phys. 2 (2000) 1051.
[65] H. Sato, S. Hasebe, H. Sakuri, K. Urabe, Y. Izumi, Appl. Catal. 29 (1987) 107.
[66] G. Dahlhoff, W. Eickelberg, W.F. Hölderich, Stud. Surf. Sci. Catal. 139 (2001) 335.
[67] G. Dahlhoff, W.F. Hölderich, in: Proceedings of the International Symposium of Zeolites and Macroporous Crystals (ZMPC), Sendai, Japan, August 6–9, 2000, abstract 2-P-083.
[68] G. Dahlhoff, U. Barsnick, W.F. Hölderich, Appl. Catal. A Gen. 210 (2001) 83.
[69] J. Röseler, G. Heitmann, W.F. Hölderich, Appl. Catal. A Gen. 144 (1996) 319.